

# Technical Report: Use of Hybrid Systems to model the Robotiq Adaptive Gripper

Giulia Franchi, Kris Hauser

School of Informatics and Computing,  
Indiana University, Bloomington

gfranchi@indiana.edu, hauserk@indiana.edu

## Abstract

This document presents a mathematical model of the states of a three-fingered robotic hand (Robotiq 3-Finger Adaptive Gripper) in quasistatic equilibrium with and without contact with an object. The mechanical coupling and the breakaway mechanism of the under-actuated robotic hand as well as its contact with the object are modeled as a hybrid system which is suitable for use for simulation, which gives rise to a kinematic model suitable for use in grasp analysis. Experiments are performed in order to verify the accuracy of the proposed model, and the model is demonstrated to produce physically plausible results in a robot physics simulator.

## 1 Introduction

Despite decades of active research, reliable grasping in unstructured environments like the home remains a major challenge in robotics. Small amounts (millimeters) of uncertainty in object shape, relative position, and robot control errors can cause grasping failure or damage to the object. One approach is to develop active adaptive behaviors that incorporate visual and tactile feedback, which requires precise sensing. Moreover, designing appropriate feedback behaviors is often challenging due to the high dimensionality of hands, which can have dozens of degrees of freedom (DOFs). An alternate approach relies on clever hardware design of passive elements, like springs, that automatically conform a hand to the shape of objects without the need for sensor feedback [1]. This approach can also greatly reduce the number of actuator elements, simplifying the control process [4–6]. Such hands are referred to as *underactuated* because there are fewer actuators than the number of degrees of freedom; each actuator drives multiple degrees of freedom in a coupled manner by complex transmission systems (tendons, gear trains, soft elements, adaptive synergies [3]. Although underactuated hands can conform to a wide variety of objects, their behavior is harder to model using traditional techniques due to nonlinear and nonsmooth coupling between degrees of freedom. Existing tools for grasp analysis and optimization (e.g., GraspIt!) fail to account for such nonlinearities, which may lead to incorrect predictions.

This Technical Report presents a model of the Robotiq 3-Finger Adaptive Gripper, a commercially available underactuated gripper with 4 actuators and 10 degrees of freedom. The gripper has a high grip strength, a resilient rigid linkage transmission system, and simple control protocol. It is currently being used in several research laboratories and by several teams in the DARPA Robotics Challenge. Although several similar research prototypes have

been studied for over a decade [1] we are not aware of existing mathematical models of the robot’s behavior suitable for simulation and optimization purposes. This report describes a quasistatic hybrid systems model of the robot suitable for such purposes. Hybrid systems model the coupled dynamics of continuous and discrete state variables, and are appropriate for dynamic discontinuities, such as those involved in contact [7]. They have been used in dexterous manipulation, see, e.g., [8] , [9], [10], [11] to model changes in contact state from no robot-object contact, to stable contact, to sliding contact. In this paper we use hybrid systems not only model changes in contact state but also the mechanical coupling and breakaway mechanism of the Robotiq gripper. For any given motor control, the model outputs the configuration of the robot in quasistatic equilibrium with a fixed object.

Extensive experiments were performed in order to compare the proposed model to the measured behavior of the physical gripper, showing accuracy within the range of measurement error. The model is also implemented in an open-source robot simulator and made available for public use.

## 2 Adaptive Gripper

The 3 finger-Robotiq Adaptive Gripper is a robotic peripheral that is designed for industrial applications [12]. It is designed to adapt to parts of varying sizes and shapes. It has three articulated fingers, i.e. finger A in front of finger B and finger C, that each have three joints (three phalanges per finger), as shown in Figure 2.1. The palm integrates four servomotors and the control electronics. Three finger phalanges are driven by one of the servomotors while the bases of fingers A and B rotate around the palm in a spread movement which is generated by the fourth servomotor.

When an inner phalange contacts an object with a certain force, a breakaway system based on a clutch decouples the outer phalange from the inner phalange so that it can perform an enveloping grasp of the object. The force value at which the breakaway system is activated is determined by torsional springs inside the phalange joints. The breakaway system is also engaged when an inner phalange reaches a joint limit (Figure 2.1). This configuration allows the underactuated fingers to automatically adapt to the shape of object they grip as the servomotor is driven to the closed position. When the outermost phalange makes contact or reaches its joint limit, the finger cannot be driven any further. The gripper controller detects this situation when the motor current rises above a certain user-defined threshold. At this point, the motor no longer driven forward and the finger remains fixed in place until a more open motor position is commanded.

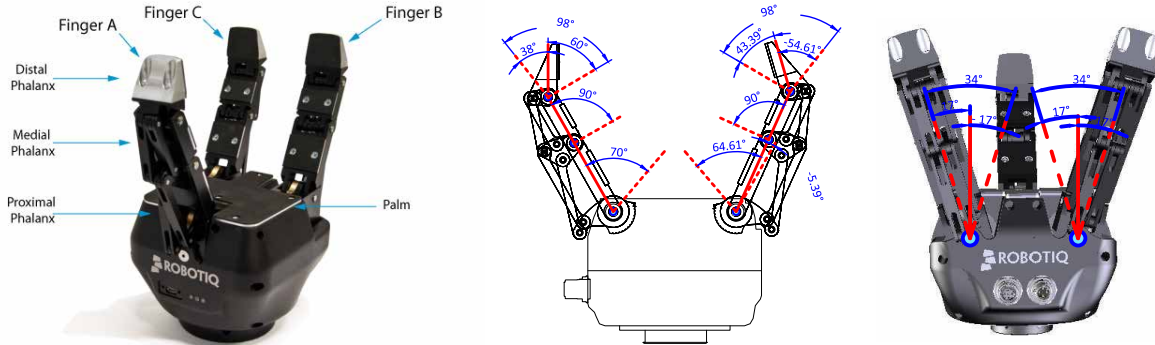


Figure 2.1: Robotiq Adaptive Gripper, S-Model (Source: Robotiq, reprinted with permission). Joint limits of the gripper.

### 3 Single finger hybrid dynamics

Hybrid systems are general mathematical models that describe the behavior of continuous dynamics and discrete events under control inputs. We first present the dynamical model of a single finger with and without an obstacle; each finger is identical so their interactions need not be modeled unless two fingers touch. In such a case the opposing finger acts as an obstacle to the first, and vice versa.

The quasistatic movement of the finger through a closing motion is described as follows.

- A gear attached to the servomotor moves a linkage in the back of the finger which presses the first phalange toward the palm through a torsional spring mechanism.
- When the movement of this phalange is blocked (either by an object or when hitting a joint stop) then a second transmission linkage presses the second phalange forward.
- When the second phalange is blocked, the third phalange moves from a similar transmission linkage.
- The third phalange eventually is blocked and closing halts.

A key assumption of our approach is that the obstacle remains in fixed position once its motion blocks any phalange (i.e., does not roll or slip). This assumption is typically justified because a gripped object only applies sufficient force to block a phalange when it is massive or it is pinned between two opposing faces of the gripper. Moreover, each finger is covered by a high friction rubber that rarely exhibits slip.

We note that our model avoids an explicit representation of the transmission linkage components in the rear of each finger. Although it may be possible to model it, the transmission is irrelevant to grasp analysis and resolving the several closed loop constraints would add significantly to the complexity of the model. Hence, we focus on the behavior of the reduced coordinates of the phalanges only.

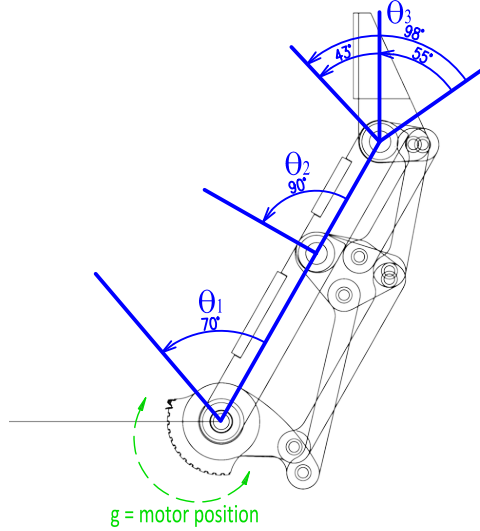


Figure 3.1: Continuous state parameters and joint limits for each finger.

The finger model describes a continuous state by the tuple:

$$x = (\Theta_1, \Theta_2, \Theta_3, g) \in [\Theta_{1,min}, \Theta_{1,max}] \times [\Theta_{2,min}, \Theta_{2,max}] \times [\Theta_{3,min}, \Theta_{3,max}] \times [0, 255] \quad (3.1)$$

where  $\Theta_1$ ,  $\Theta_2$ , and  $\Theta_3$  are the relative joint angles of each phalanges with respect to the proximal parent, and  $g$  is the reference position of the servomotor. The control input

$$u \in [-1, 1] \quad (3.2)$$

describes the change in  $g$  from one time step to another during normal operation. In the controller's fixed-precision implementation  $g$  and  $u$  are integer values, but we model them as continuous values for simplicity.

We also define four discrete *movement phases* of the finger:

1. The first phalange moves freely, the second stays extended, and the third moves opposite the first to maintain a vertical orientation.
2. The first phalange is blocked, the second phalange moves, and the third moves opposite the second to maintain a vertical orientation.
3. The second phalange is blocked, and the third link moves.
4. The third phalange is blocked, and the finger freezes.

We denote a similar phases 1' and 2', wherein the third phalange hits its lower joint limit of  $-55^\circ$  and cannot maintain a vertical orientation.

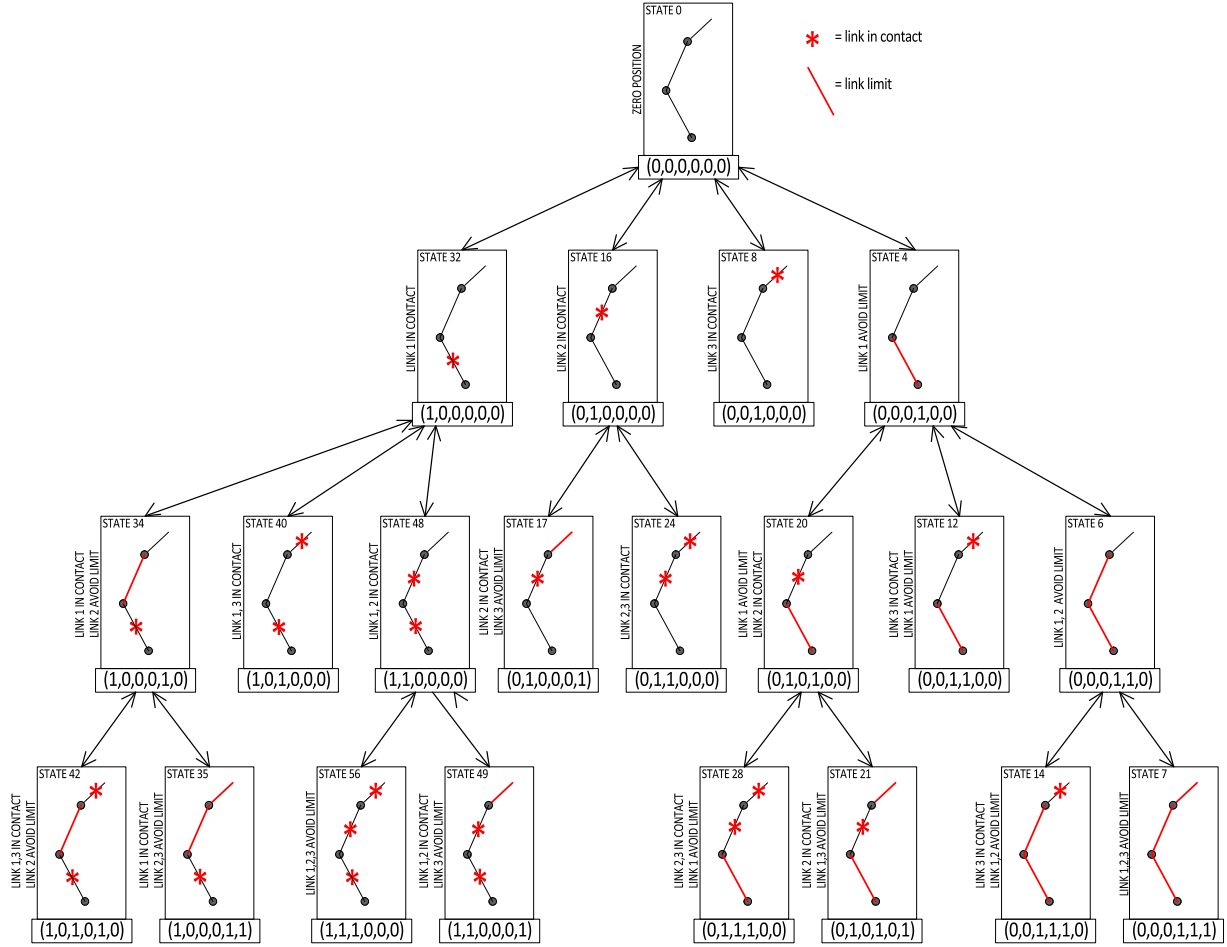


Figure 3.2: Representation of the possible discrete states for one finger

Considering that a blockage can be caused by both an object (which occurs at variable position) as well as a joint limit, we consider these as different states in the hybrid system. A labeling for all possible discrete states of one finger is shown in Figure 3.2.

A discrete state is a tuple  $(c_1, c_2, c_3, l_1, l_2, l_3)$  of binary variables, where

$c_i = 1$  indicates movement of link  $i$  is blocked by contact with an object.

$l_i = 1$  indicates movement of link  $i$  is blocked by its upper joint limit, i.e.,  $\Theta_i = \Theta_{i,max}$ .

$l_3 = -1$  indicates reverse movement of link 3 is blocked by its lower joint limit, i.e.,  $\Theta_3 = \Theta_{3,min}$ .

We remark that not all discrete states are reachable, for example, any state with  $c_i = l_i = 1$  for any  $i = 1, 2, 3$  are not possible. For each state  $(c_1, c_2, c_3, l_1, l_2, l_3)$  we can describe  $\Delta\Theta$  and  $\Delta g$  as a function of  $x$  and  $u$ .

Phase	State tuples	$\Delta\Theta_1$	$\Delta\Theta_2$	$\Delta\Theta_3$	$\Delta g$
1	(0, 0, 0, 0, 0, 0)	$f_1(x, u)$	0	$-f_1(x, u)$	$u$
1'	(0, 0, 0, 0, 0, -1)	$f_1(x, u)$	0	0	$u$
2	(1, 0, 0, 0, 0, 0), (0, 0, 0, 1, 0, 0)	0	$f_2(x, u)$	$-f_2(x, u)$	$u$
2'	(1, 0, 0, 0, 0, -1), (0, 0, 0, 1, 0, -1)	0	$f_2(x, u)$	0	$u$
3	( $\cdot$ , 1, 0, $\cdot$ , 0, 0), ( $\cdot$ , 0, 0, $\cdot$ , 1, 0)	0	0	$f_3(x, u)$	$u$
4	( $\cdot$ , $\cdot$ , 1, $\cdot$ , $\cdot$ , 0), ( $\cdot$ , $\cdot$ , 0, $\cdot$ , $\cdot$ , 1)	0	0	0	0

where:

$$f_1(x, u) = m_1 u, \text{ with } m_1 = \Theta_{1,max}/140$$

$$f_2(x, u) = m_2 u, \text{ with } m_2 = \Theta_{2,max}/100$$

$$f_3(x, u) = m_3(g)u, \text{ with } m_3(g) = \Theta_{3,min} + (\Theta_{3,max} - \Theta_{3,min})/(255 - g)$$

Transition conditions are given as follows.

1.  $c_i = 0 \rightarrow c_i = 1$ : an object is hit by link  $i$ .
2.  $c_i = 1 \rightarrow c_i = 0$ :  $\Theta_{i+1} = \Theta_{i+1,min}$  and  $u < 0$ .
3.  $l_i = 0 \rightarrow l_i = 1$ :  $\Theta_i + \Delta\Theta_i \geq \Theta_{i,max}$ .
4.  $l_i = 1 \rightarrow l_i = 0$ :  $\Theta_i + u < \Theta_{i,max}$ .
5.  $l_3 = 0 \rightarrow l_3 = -1$ :  $\Theta_3 + \Delta\Theta_3 \leq \Theta_{3,min}$ .
6.  $l_3 = -1 \rightarrow l_3 = 0$ :  $\Theta_3 + u > \Theta_{3,min}$ .

A state machine depiction of the finger hybrid system is given in Figure 3.3. To obtain a general hybrid system for the hand with just put together the three state machine scheme for one finger.

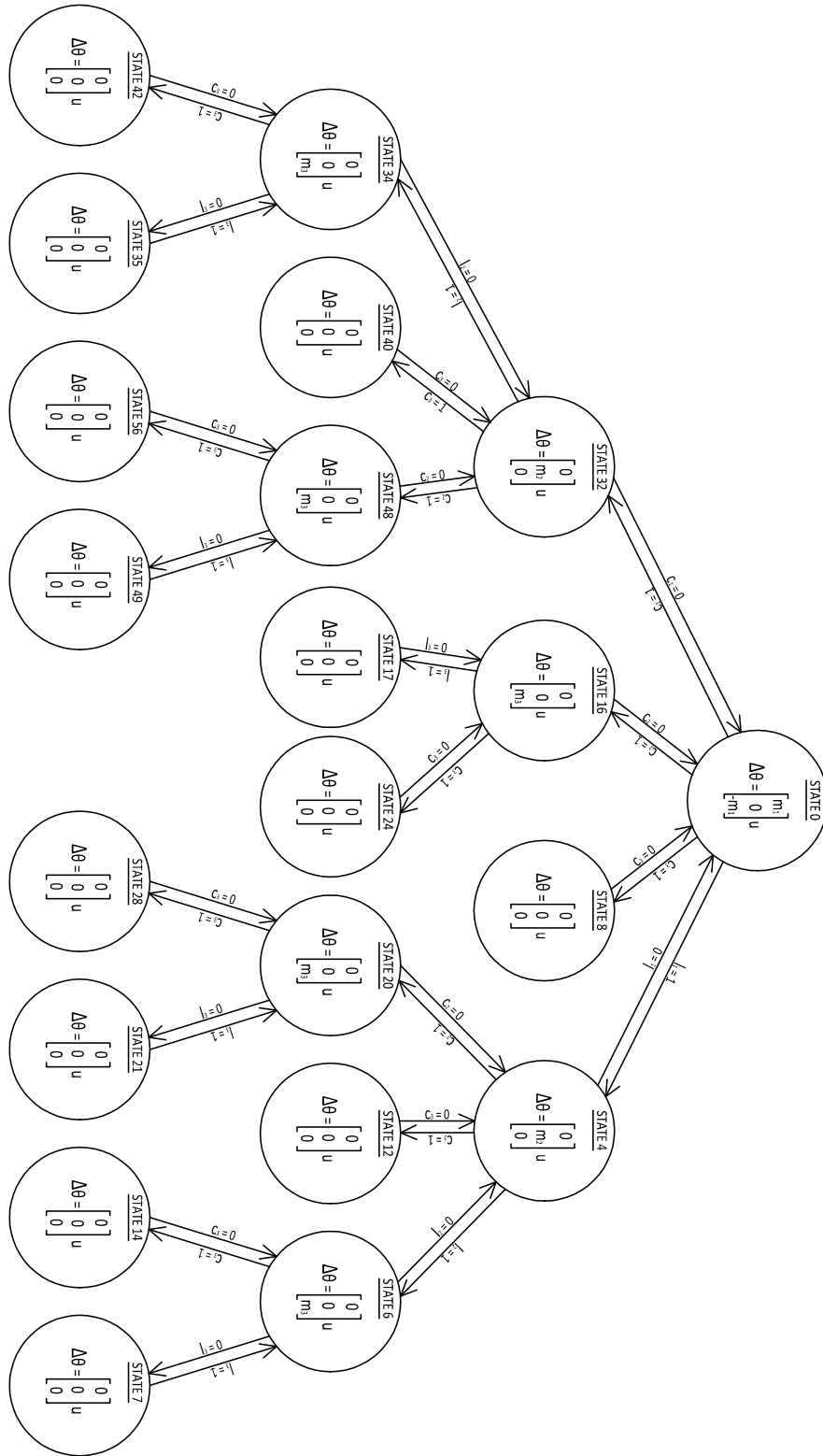


Figure 3.3: State Machine representation for one finger hybrid system

## 4 Analytical model of one finger and one-link contact

The hybrid system model gives a dynamic equation that is useful for forward simulation but is not as useful for analysis, where one may want to quickly determine the finger configuration when the servomotor is driven to a particular value. Here we determined analytically the unique state corresponding to a particular value of  $g$  in the absence of obstacles. Moreover, if one knew the value of  $g$  where the obstacle would first be touched, a unique state for a given  $g$  can also be determined quickly. In future work, we are interested in using these equations for grasp analysis and optimization.

### 4.1 Analytical Equations without Object

Here we derive the joint angle equations in the absence of an object causing blockage. Joint limits are incorporated here. In this table, define the constants  $m_1 = \Theta_{1,max}/140$  and  $m_2 = \Theta_{2,max}/100$ .

Phase	Motor range	$\Theta_1$	$\Theta_2$	$\Theta_3$
1	$0 \leq g \leq 110$	$m_1g$	0	$-m_1g$
1'	$110 < g \leq 140$	$m_1g$	0	$\Theta_{3,min}$
2	$140 < g \leq 240$	$\Theta_{1,max}$	$m_2(g - 140)$	$\Theta_{3,min}$
4	$240 < g \leq 255$	$\Theta_{1,max}$	$\Theta_{2,max}$	$\Theta_{3,min}$

The stoppage at  $g = 240$  is due to self-collision with the finger and the palm. Note that we can also express the behavior of  $\Theta_3$  in Phases 1 and 1' in the form  $\Theta_3 = \max(-m_1g, \Theta_{3,min})$ .

### 4.2 Analytical Equations with Object

Suppose  $g_{ob}$  is the motor position in which any link of the finger is first blocked by the object. As the finger closes, we can integrate the equations of motion to determine the link behavior for  $g > g_{ob}$ . In the below tables, let us define the constant  $c = \Theta_{3,max} - \Theta_{3,min}$ . The derivation of the following equations is straightforward except for the behavior of  $\Theta_3$ , which is non-linear in Phase 3. From experimental data, we observed that  $\Theta_3$  reaches its limit when  $g$  is halfway between 255 and the value of  $g$  when  $\Theta_2$  stops moving (see Fig 4.1). This equation also fits the slight curve observed in the data.

The following table governs behavior for contact made only on the **first link**:

Obs. range	Motor range	$\Theta_1$	$\Theta_2$	$\Theta_3$
$g_{ob} \leq 140$	$0 < g - g_{ob} \leq 100$	$m_1g_{ob}$	$m_2(g - g_{ob})$	$\max(-(\Theta_1 + \Theta_2), \Theta_{3,min})$
$g_{ob} \leq 140$	$g - g_{ob} > 100$	$m_1g_{ob}$	$\Theta_{2,max}$	$\min(\Theta_{3,max}, \Theta_{3,min} + (\frac{c(g-g_{ob}-100)}{255-g}))$

This table governs behavior for contact made only on the **second link**:

Obs. range	Motor range	$\Theta_1$	$\Theta_2$	$\Theta_3$
$g_{ob} \leq 140$	$g_{ob} < g$	$m_1g_{ob}$	0	$\min(\Theta_{3,max}, \Theta_{3,min} + (\frac{c(g-g_{ob})}{255-g}))$
$140 < g_{ob}$	$g_{ob} < g$	$\Theta_{1,max}$	$m_2(g_{ob} - 140)$	$\min(\Theta_{3,max}, \Theta_{3,min} + (\frac{c(g-g_{ob})}{255-g}))$

When **both link 1 and link 2 make contact**, only the third link can move. Let  $g_{ob1}$  and  $g_{ob2}$  be the motor position in which link 1 and link 2 are blocked by the object. They

must satisfy  $g_{ob1} \leq 140$  and  $0 < g_{ob2} - g_{ob1} \leq 100$ . In this case, the third link's behavior is governed by the equation  $\Theta_3 = \min(\Theta_{3,max}, \Theta_{3,min} + (\frac{c(g-g_{ob2})}{255-g}))$ .

Finally, when the **third link makes contact**, the gripper stops moving.

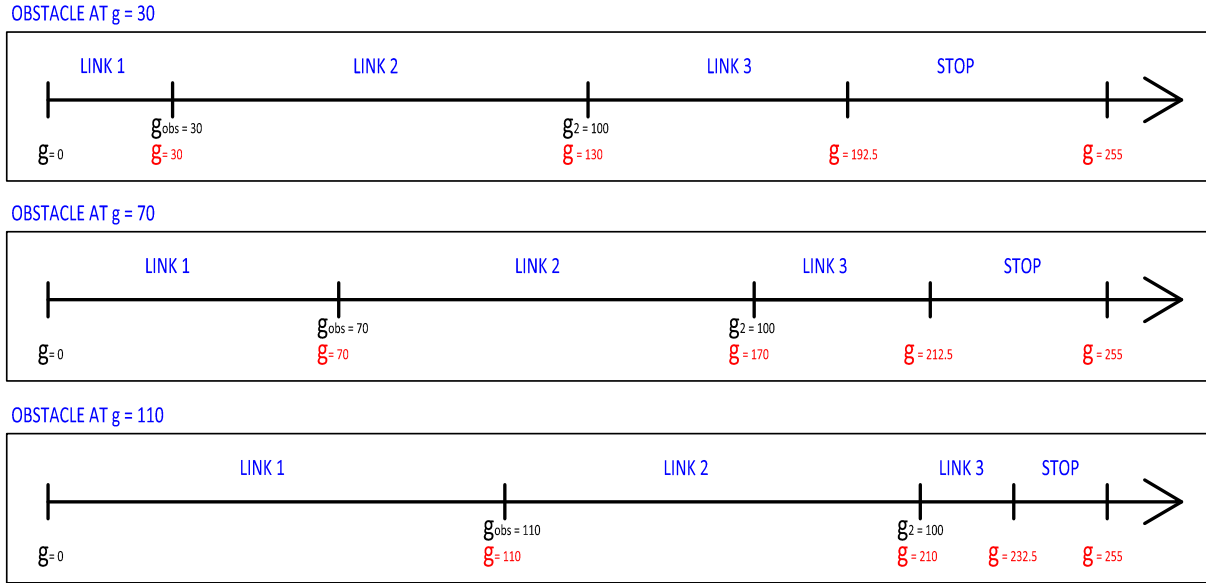


Figure 4.1:  $\Theta_3$  stopping condition: experiments demonstrate that it hits its limit when  $g$  reaches halfway between the stopping point of  $\Theta_2$  and 255.

## 5 Experimental Validation

We verify the motion model of the gripper by moving the gripper through a sequence of configurations and comparing joint angle predicted by the model for each configuration with the joint angle measured empirically. This is difficult because the joints do not have angular encoders. Instead an external visual tracking apparatus was devised.

### 5.1 Visual Tracking Measurement

We attach fiducial markers to each joint such that the markers are centered on the joint (Figure 5.1). We then recorded the 3D position of each marker in the workspace using data provided by an RGB+D camera. The markers are tracked using color blob tracking on the 2D image provided by the camera. The blobs are tracked as axis-aligned bounding rectangles on the image, and the blob tracker provides both the center coordinates and bounds of each blob (in pixels), along with its detected color.

The blob tracker is based on the CMVision library, which is described in [16] (see [17] too). One method to compute the 3D positions of each joint would be to use the center coordinates of each blob to index into the organized point cloud (see [14]) provided by the



Figure 5.1: Visual Tracking with RGB+D

camera and retrieve the corresponding point. In practice, however, this often results in invalid points because the depth computation may have failed to result in a valid value for that particular pixel. Instead, the following procedure is used to compute 3D positions:

1. Color blobs corresponding to the fiducial markers are detected in the 2D image.
2. All valid points in the corresponding point cloud that fall within the bounding rectangle of the blob are retrieved.
3. Statistical outlier removal (see [15]) is performed to filter points that are unlikely belong to the marker.
4. The centroid of the remaining points is taken as the center of the fiducial marker.
5. We know from the construction of the gripper that the joints are all co-planar, so a plane is fit to the set of centroids representing joint positions in the workspace, and those centroids are projected onto that plane.
6. Finally, we know also that all joints have parallel axes of rotation, thus, given the absolute positions of the joints in space, we can construct vectors between them and compute the joint angles explicitly using the definition of the dot product.

It was also helpful to extend step 2 to accumulate data over a user-defined number of frames generated by the camera. This reduced the effect of camera noise and resulted in more stable readings; for these experiments, a window of 25 frames was used.

We collected angles at each integer step of  $g$  ranging from 0 to 255 (full closed to fully open). Noise in the measurement process sometimes produced outliers, particularly for link 3, because the distance from one marker to the next is smaller than that of any other joints. So, we employed an outlier removal process. We considered an outlier to be a change in sensed angle that is more than 5 degrees from one value of  $g$  to the next (which certainly

does not actually occur on the physical robot). We limited the measurement to be within  $\pm 5$  degrees of the previous and next inlier points.

## 5.2 Validation

First, the model was tested without an object (Fig 5.2) in five experiments.

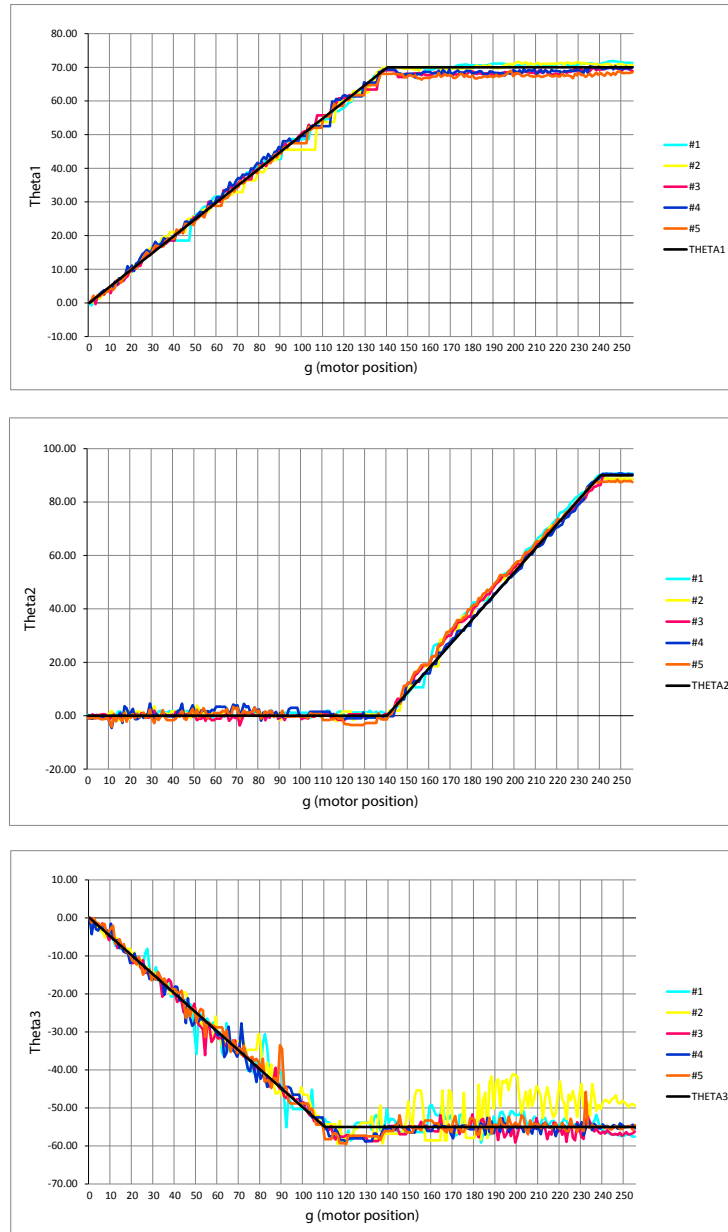


Figure 5.2: Comparing model to measured behavior of  $\Theta_1$ ,  $\Theta_2$ , and  $\Theta_3$  in 5 runs without obstacles.

We tested the model accuracy analyzing the Mean Square Error (MSE) of the model, the MSE of the data, the Mean Standard Deviation (MSD) of the model and the MSD of the data.

Data Analysis				
	MSE		MSD	
Angle	Model	Data	Model	Data
$\Theta_1$	0.74	1.41	0.50	0.68
$\Theta_2$	2.00	1.70	0.70	0.72
$\Theta_3$	1.93	6.25	0.75	1.24

This table demonstrates that the model has comparable accuracy to the measurement accuracy on link 2 and is well within measurement accuracy for links 1 and 3.

Next, we tested the model with objects of varying position. We calculate  $g_{ob}$  as the motor position in which the finger first contacts the object. The object is a fixed rigid bar with adjustable position in a box rigidly attached to the robot's base (Figure 5.3).

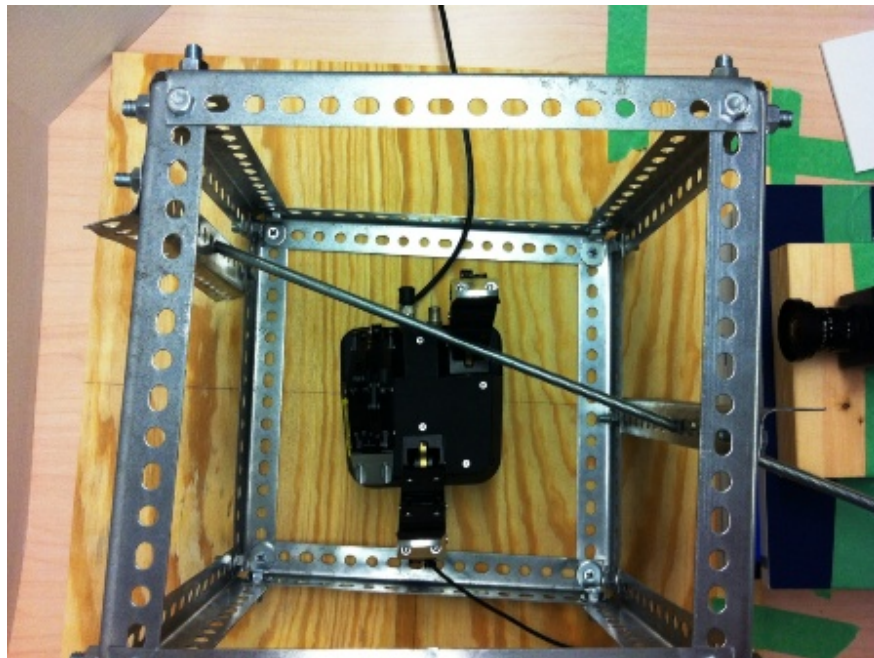


Figure 5.3: Experiment environment

## 6 Simulation Model Implementation

After testing the mathematical model through the observation of the real behavior of the gripper, we implemented it in the Klamp't robot simulator [13] (Figure 6.1). This is a physics simulation that simulates contact forces and joint torques. The joint angles outputted by our model are inputted into the system as reference values for PID controllers in the phalange

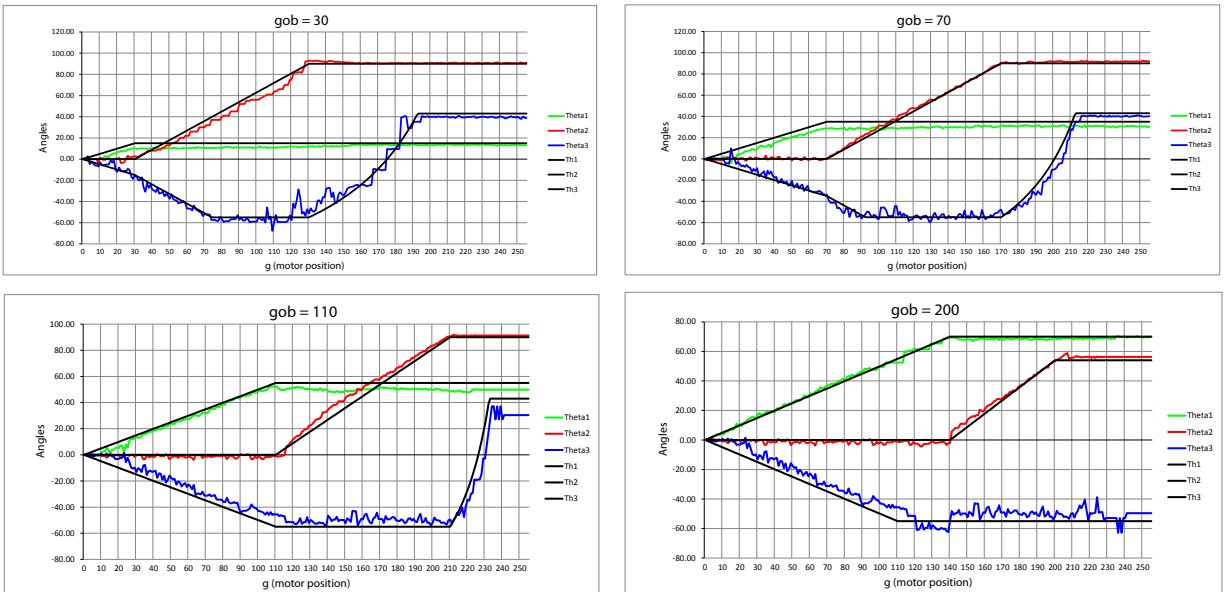


Figure 5.4: Experiment with an object in positions  $g_{ob} = 30$ ,  $g_{ob} = 70$ ,  $g_{ob} = 110$ , and  $g_{ob} = 200$ .

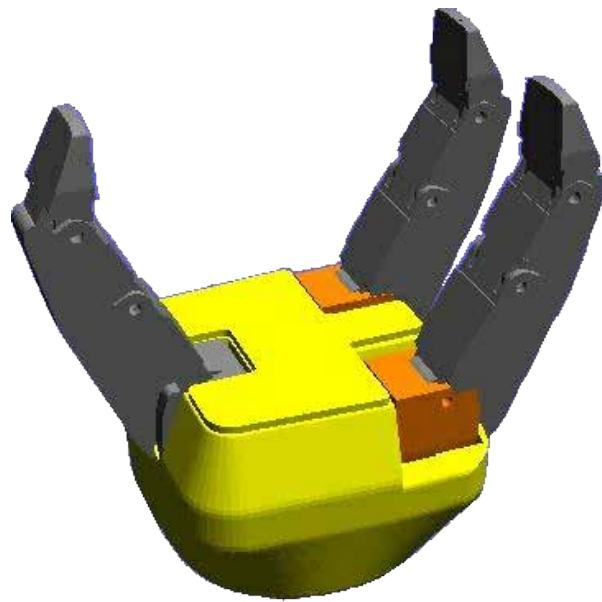


Figure 6.1: Geometrical Model in Klamp't environment

joints. Fig. 6.2 shows different picture with progressive value of  $g$  during a simulation without object.

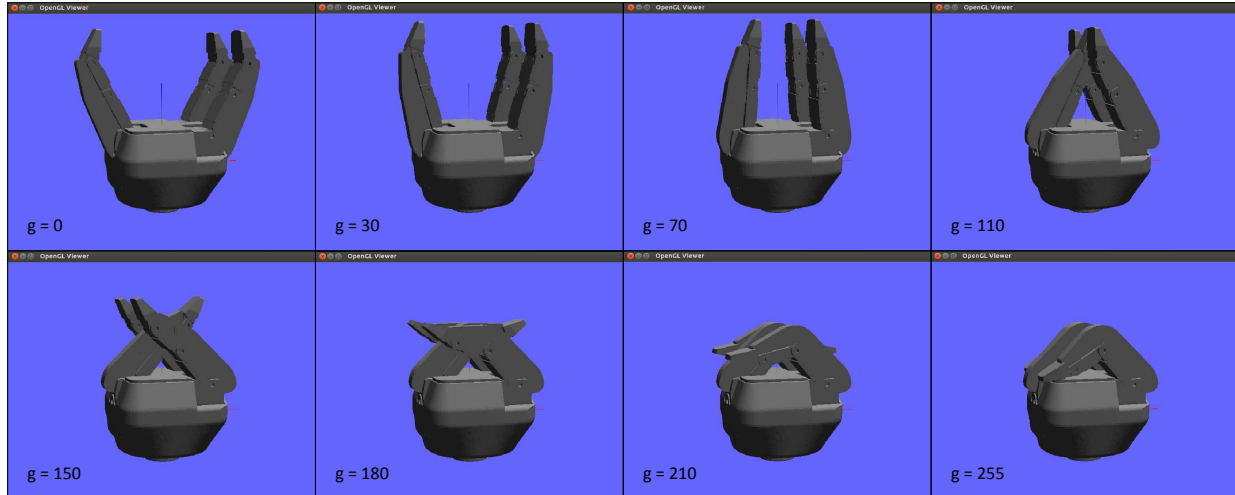


Figure 6.2: Simulation without object

## 6.1 KLAMPT Model Test with object

Hereinafter some significant simulations to test the Klampt model with object are presented. Observe that in the simulation with  $g_{ob} = 160$  a picture of the real experiment is shown. The object set in the simulation environment is a long and thin cylinder and it's considered a fix object. This scenario was prepared to compare the simulation with the real experiment we made on the real gripper using the metallic box.

## 7 Conclusion

A hybrid system model of an underactuated robotic hand is presented, both in the form of dynamic equations and their analytical solutions. The model is verified with a vision-based data collection system to match the experimental data well within measurement error. The model is implemented in a demo program in Klampt, which is freely available from <http://klampt.org>. In future work we wish to perform a more precise empirical validation and to implement the model for grasp optimization and object recognition without additional sensors. We also intend to build a more complete model of the force characteristics of the gripper in contact with an object.

## References

- [1] C.M. Gosselin and T. Lalibertè, *Underactuated Mechanical Finger with Return Actuation*, U.S. Patent 5 762 390, 1998.
- [2] C. Melchiorri and M. Kaneko, *Robotic Hand*, pp. 345-360 (B.Siciliano and O. Khatib, Eds, Handbook of Robotics. Berlin: Spinger, 2008).

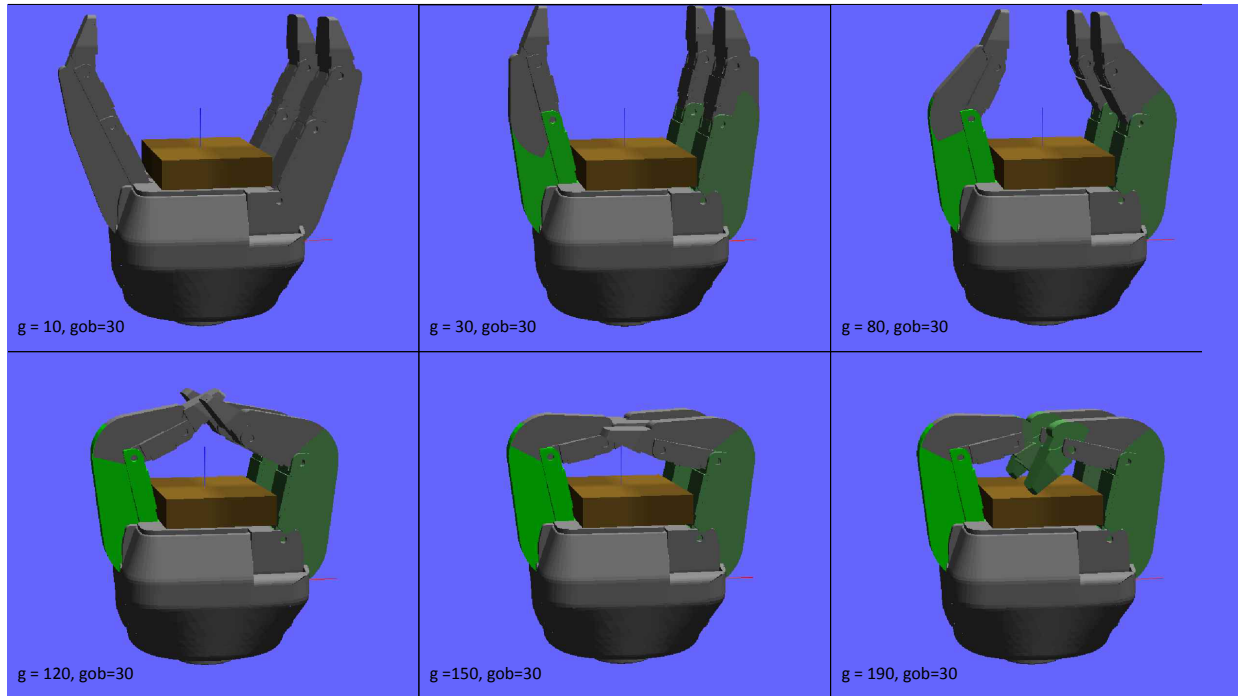


Figure 6.3: Simulation with object: gob = 30

- [3] M.G. Catalano, G. Grioli, A. Serio, E. Farnioli, C. Piazza and A. Bicchi, *Adaptive Synergies for a Humanoid Robot Hand*, IEEE-RAS International Conference on Humanoid Robots, 2012.
- [4] L. Birglen, T. Lalibertè and C. Gosselin, *Underactuated robotic hands*, pp. 345-360 (B.Siciliano and O. Khatib, F. Groen, Eds, Springer Tracts in Advanced Robotics. Berlin: Spinger, 2008).
- [5] W. Townsend, *The BarrettHand grasper - programmably flexible part handling and assembly*, vol. 27 (3), pp. 181-188 (Ind. Rob., 2000).
- [6] T. Lalibertè, L. Birglen and C.M. Gosselin, *Underactuation in robotic grasping hands*, Machine Intelligence and Robotic Control, Vol. 4, No. 3, 1-11 (2002).
- [7] S. Engell, G. Frehse and E. Schnieder (Eds.), *Modeling, Analysis and Design of hybrid Systems*, pp. 436-465 (T. Schlegl, M. Buss and G. Schmidt, Hybrid Control of Multi-fingered Dextrous Robotic Hands), 2002.
- [8] T. Schlegl, M. Buss and G. Schmidt, *A Hybrid Systems Approach Toward Modeling and Dynamical Simulation of Dextrous Manipulation*, IEEE/ASME Transaction on Mechatronics, 2003.

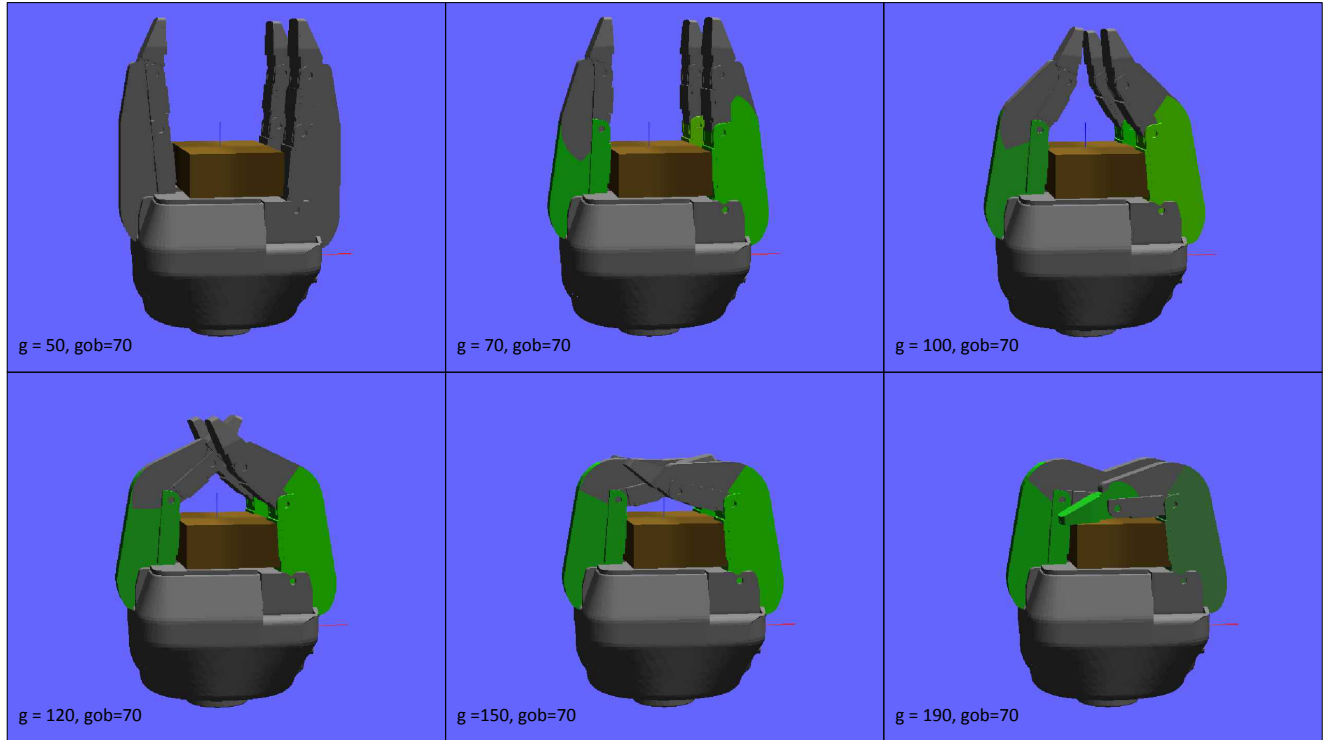


Figure 6.4: Simulation with object: gob = 70

- [9] Y. Yin, M. Svinin and S. Hosoe, *Modeling and control of multifingered robot hand for dexterous manipulation: a continuous and discrete hybrid approach*, Systems, Man and Cybernetics, IEEE International Conference, 2004.
- [10] T. Schlegl and M. Buss, *Dextrous hand regrasping using Hybrid System Models*, Advanced intelligent Mechatronics, Tokyo, 1997.
- [11] S.L. Ricker, N. Sarkar and K. Rudie, *A discrete-event systems approach to modeling dextrous manipulation*, vol 14, pp.515-525, Robotica, 1996.
- [12] <http://robotiq.com/en/products/industrial-robot-hand>, (Technical sheets), (accessed Sep.10, 2013)
- [13] <http://www.indiana.edu/~motion/software.html>, (accessed Jan.28, 2014)
- [14] <http://www.pointclouds.org/documentation/tutorials/basic\textunderscorestructures.phpbasic-structures>, (accessed Oct.5, 2013)
- [15] <http://pointclouds.org/documentation/tutorials/statistical\textunderscoreoutlier.php>, (accessed Oct.5, 2013)

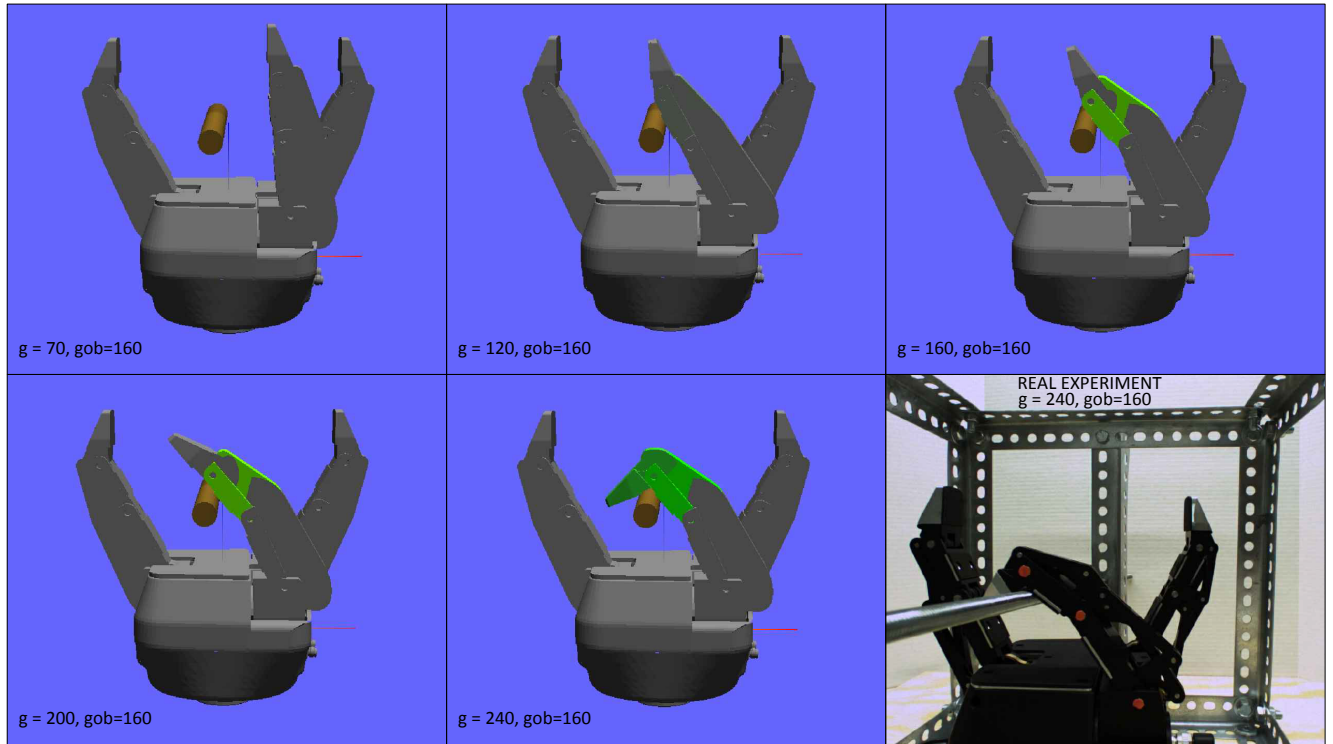


Figure 6.5: Simulation with object: gob = 160

- [16] J. Bruce, T. Balch and M. Veloso *Fast and inexpensive color image segmentation for interactive robots*, IEEE/RSJ International Conference on intelligent Robots and Systems, 2000 (IROS 2000).
- [17] <http://wiki.ros.org/cmvision/textunderscoreoutlier.php>, (accessed Oct.5, 2013)